PAPER

Check for updates

Experimental study on the variation of coal pore structure under the coupling effect of oxidation temperature and duration

Yaxian Yu,[a] Zhenya Zhang, [ID] *[ac] Song Kong[b] and Peitao Zhu [ID] [a]

To elucidate the evolution of coal pore structure under coupled temperature–time effects, this study conducted programmed temperature oil-bath experiments to treat coal samples under varying thermal conditions. The pore characteristics, including pore volume, specific surface area, and pore size distribution, were systematically analyzed through low-temperature nitrogen adsorption (LTNA) measurements and BET theory. Furthermore, the FHH fractal theory was employed to quantitatively characterize the pore structure heterogeneity. The results indicate that the shape of the coal adsorption–desorption curves remained largely unchanged with increasing heating temperature and duration. In terms of pore volume distribution, the mesopore fraction exhibited a consistent decreasing trend, the micropore fraction initially declined before increasing, while the macropore fraction exhibited an initial increase followed by a subsequent reduction. Regarding the surface area distribution, the proportion of mesopores and macropores exhibited an initial decrease followed by an increase, whereas the micropore fraction demonstrated a converse trend, increasing first and subsequently decreasing. The fractal characteristics of pores are significant, with the fractal dimension $D_1 > D_2$ indicating that the surface pores exhibit rougher structures compared to the internal pore network. Under fixed heating duration, the elevation of temperature lead to concurrent decreases in both D_1 and D_2 values. When maintaining constant temperature conditions, the value of D_1 demonstrated an initial decline followed by recovery, while that of D_2 showed a trend of initial increase and subsequent reduction. This reveals the dynamic evolutionary process of pore structure.

1. Introduction

The coal matrix exhibits a complex pore structure, whose intricate network provides migration pathways for adsorbed gas stored within the coal seam. The heterogeneity of pore structures governs the storage and migration mechanisms of coalbed methane.[1–6] Consequently, investigating the evolution of coal microstructure and its fractal characteristics holds significant implications for coalbed methane (CBM) resource exploitation. To further explore the microstructural pore characteristics of coal, scholars have conducted research on the pore development characteristics.[7–10]

Zhou *et al.*[11] conducted a study on low rank coals with different macroscopic coal-rock types, explored the adsorption pore characteristics of low-rank coals, and pointed out the correlation between fractal dimension and both pore structure

and adsorption performance. Their findings demonstrated that the adsorption process of low-rank coals undergoes a distinct transition from monolayer-dominated to multilayer-dominated adsorption with increasing pressure. Li *et al.*[12] conducted a comparative analysis of the pore structure in medium-rank coal using mercury intrusion porosimetry (MIP) and liquid nitrogen adsorption methods (LTNA). By employing both Menger and FHH models to investigate fractal characteristics, they demonstrated that surface area and pore volume exhibit a nonlinear concave curve with increasing burial depth, and the fractal dimension shows a convex curve trend, which reveals a dynamic correlation between pore structure complexity and burial depth. Liu *et al.*[13] investigated the evolutionary patterns of pore structures in medium and high rank coals, and explored the characteristics of pore structure and fractal properties of different coal ranks. The results demonstrated the surface roughness was positively correlated with the coal grade. To investigate the impact of pore heterogeneity on CBM storage and migration in reservoirs, Zhang *et al.*[14] characterized the pore structure and fractal features of high-rank coal from the Nuodong area (Southwest Guizhou) through MIP and LTNA experiments. The results indicate that the coal reservoir is predominantly microporous, with pronounced fractal

[a]Zhejiang Key Laboratory of Intelligent Construction and Operation & Maintenance for Deep-Sea Foundations, Ningbo University of Technology, Ningbo, 315211, P. R. China. E-mail: zhangzhenya@nbut.edu.cn

[b]Zhejiang Institute of Tianjin University, Ningbo, 315211, China

[c]Liaoning Technical University Liaoning Key Laboratory of Mining Environment and Disaster Mechanics, Fuxin, Liaoning 123000, China

characteristics. Pore heterogeneity intensifies with increasing coal rank, while the content of vitrinite and inertinite exhibits a negative correlation with fractal dimension. Through adsorption–desorption experiments, Yin et al.[15] characterized the evolution of pore structures during pyrolysis across different coal ranks. Their results indicate that elevated temperatures may induce framework melting and collapse, leading to diminished adsorption capacity.

Zhang et al.[16] investigated the effects of high-pressure CO_2 adsorption/desorption on the pore structures of lean coal, 1/3 coking coal, and gas coal through low-temperature N_2 and low-pressure CO_2 adsorption experiments. The results revealed that while the pore morphology remained unchanged, the nanoscale pore size was co-regulated by adsorbed and free gas phases. All three coal types exhibited reduced hysteresis loops, a shift in pore size distribution toward smaller dimensions, increased micropore proportion, and enhanced pore connectivity. Zhao et al.[17] carried out a research on the nanoscale pores of anthracite by combining nitrogen adsorption and MIP, characterized and analyzed the pore structure and the influence on gas behavior. Their findings suggested that nanoscale pores have poor connectivity and low permeability, which affects the production of coalbed methane. Qi et al.[18] took the deep coking coal in Pingdingshan No. 12 Coal Mine as the research object, and combined with LTNA and MIP to carry out experiment on its soft and hard coal. They concluded a polarized pore distribution pattern characterized by predominant macropores, scarce mesopores, and intricately structured micropores. Lin et al.[19] conducted research on coals of different metamorphic degrees and different coal structures, and explored the characteristics of the pore size distribution and pore structure of the micro-pores in coal.

Li et al.[20] investigated the effects of microwave heating on coal rock properties through integrated simulation, experimentation, and analysis. Their results demonstrated that microwave heating expands and interconnects pores and fractures within coal, thereby effectively enhancing pore structure. Furthermore, they employed nuclear magnetic resonance (NMR) multifractal theory to quantify linear relationships between adsorption fractal dimensions and temperature, as well as between seepage fractal dimensions and thermal heterogeneity. Cui et al.[21] employed N_2 adsorption and fractal theory to elucidate the evolution of semicoke pores during coal pyrolysis and its impact on volatile mass transfer. A particle-scale pyrolysis model was established, revealing that mesopores dominate the pore structure, with their evolution governed by degassing, cracking, and shrinkage. Additionally, micropores enhance structural heterogeneity, while pore networks significantly alter volatile yields by regulating tar diffusion. Zhou et al.[22] conducted pyrolysis treatment on anthracite samples through uniaxial compression tests and MIP, revealing that 300 °C serves as the threshold temperature for pore structure transformation, with macropores dominating the evolutionary behaviour.

Previous studies have mainly focused on the effects of regional variations, coal ranks, metamorphic degree, or individual heat treatment factors on the microscopic pore structure.

However, research on the coupled influence of temperature and time as dual variables remains limited. In this study, liquid nitrogen adsorption experiments and BET measurements were employed to analyze the pore morphology, size distribution, volume, and specific surface area of coal samples subjected to high-temperature heat treatment under varying durations. This approach systematically elucidates the synergistic mechanisms governing pore evolution during dynamic thermal processes. To further investigate, the concept of fractal dimension was introduced, integrating FHH fractal theory[23,24] with BET multi-scale analysis to quantitatively characterize pore complexity and surface roughness. A quantitative model linking pore roughness to mass transfer efficiency was established, exploring the evolution of microscopic pore structure and fractal features under coupled temperature–time effects. The results demonstrate a nonlinear interaction between temperature and duration in pore evolution, suggesting the mechanisms of micropore proliferation and mesopore reconstruction. These findings provide a theoretical foundation for optimizing coalbed methane resource extraction.

2. Experimental approaches and classification of coal pores

2.1 Selection of coal samples

The coal samples used in the study were bituminous coal from the Yilan Third Coal Mine in Yilan County, Heilongjiang Province. The industrial analysis results of the raw coal samples are presented in Table 1. The experimental treatment conditions and the nomenclature of the coal samples are presented in Table 2.

Table 1 Industrial analysis results of coal samples

Mad/%	Aad/%	Vad/%	FCad%
9.58	5.08	39.50	45.84

Table 2 Experimental treatment conditions and nomenclature for coal samples

Variable indicators 1: heat treatment temperature (°C)	Variable indicators 2: heat treatment time (min)	Notation
Untreated	Untreated	R_C
70	30	A_1
	60	A_2
	120	A_3
110	30	B_1
	60	B_2
	120	B_3
140	30	C_1
	60	C_2
	120	C_3

1-Oxygen cylinder；2-Nitrogen cylinder；3-Flow rate meter；

4-U shaped tube；5-Reticular screen mesh；6-Silicon oil；7-Control panel；

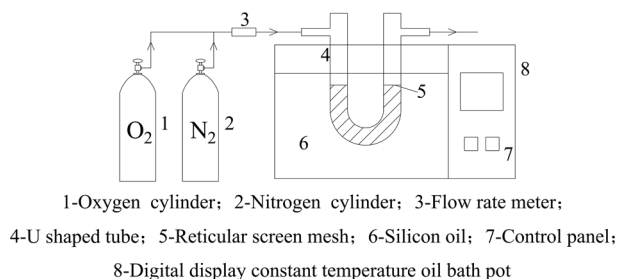8-Digital display constant temperature oil bath pot

Fig. 1 Experimental system for heat treatment of coal samples.

2.2 Process of heat treatment experiment

This test adopted programmable temperature-controlled oil bath test device equipped and made use of its intelligent temperature regulation unit to preset and maintain temperature. Silicone oil was used as the heat transfer medium, which has a high specific heat capacity and can quickly and uniformly transfer heat to the coal samples to ensure stability during the experimental process.

The experimental system includes: (1) gas supply system: including gas cylinder and gas flow meter; (2) heating/constant temperature system: including U-shaped tube and constant temperature oil bath pot; (3) temperature data acquisition system. As shown in Fig. 1.

During the experiment, the coal samples was loaded into a slender cylindrical U-shaped tube (as shown in Fig. 2(a)). The tube was equipped with gas inlet and outlet ports at both ends. To prevent the tubes from being clogged by coal powder during the experiment, mesh screens and cotton balls were set at both ends of the tube. The heat treatment was carried out at 70 °C, 110 °C, 140 °C, and 170 °C respectively, and each heat treatment temperature was conducted for 30 minutes, 60 minutes, and 120 minutes respectively.

After the oil bath reached the set temperature and stabilized for 30 minutes, the U-tube containing the coal sample was immersed in the oil bath, and connected it to oxygen. The technical specifications of the oil bath apparatus are provided in Fig. 2(b) and Table 3.

During the heating process, the weight was measured at 10-minute intervals. After the treatment reached the predetermined time, oxygen supply was terminated and replaced with nitrogen to halt further oxidation. Then, the U-tube was extracted from the oil bath and subsequently cooled to ambient temperature. Subsequently, both the reaction products and the empty tube were weighed. After weighing, the sample was dried together with the raw coal at 120 °C for 5 hours under vacuum conditions, then cooled them to room temperature in a vacuum environment. Finally, sealed and stored the coal sample in zip-lock bags and record it, in which the raw coal samples were numbered R_C.

2.3 Principles and methodology of low-temperature nitrogen adsorption

This study characterizes the microporous structure of coal through low-temperature nitrogen adsorption (LTNA) at 77 K (−196 °C). At this cryogenic temperature, gas adsorption on solid surfaces is significantly enhanced. During the experiment, nitrogen gas flows through the solid adsorbent material and becomes adsorbed onto the internal surfaces of coal pores. The relevant sample parameters were derived from the relationship between adsorption quantity and relative pressure.[25,26]

Table 3 Technical parameters of the digital display constant temperature oil bath pot

Instrument model	HH-S50
Temperature control range (°C)	Ambient +5–300
Temperature resolution (°C)	±1
Temperature fluctuation (°C)	±1
Temperature uniformity (°C)	±1
Heating power (W)	800 W
Bath dimensions (mm)	$\Phi 220 \times 120$ (diameter × depth)

Table 4 Technical parameters of ASAP2460 aperture analyzer

Instrument model	ASAP 2460
Pore size detection range (nm)	0.35–500
Specific surface area measurement range (m² g⁻¹)	≥0.0005
Pore volume resolution (cm² g⁻¹)	0.0001

(a) U-shaped tube   (b) Digital Constant Temperature (Oil) Bath   (c) the ASAP2460 aperture analyzer

Fig. 2 Actual picture of key instruments.

Table 5 Classification of coal pore systems

Scholar	Micropore/nm	Ultramicropore/nm	Transitional pore/nm	Ostiole/nm	Mesopore/nm	Macropore/nm
Hodot (1966)[28]	<10			10–100	100–1000	10^3–10^5
GAN (1972)[29]	0.4–1.2		1.2–30			30–2960
Dubinin (1974)[30]	<1.3	1.3–3.1			3.1–300	>300
Wu Jun (1991)[31]	<10		10–100		100–1000	1000–1500
Liu changhong (1993)[32]	<10		10–100		100–7500	>7500
Qin Yong (1995)[33]	<15			15–50	50–400	>400
Fu Xuehai (2005)[34]	<8				65–325	1000
Ju Yiwen (2005)[35]	5–15		15–100			
Sang Shuxun (2005)[36]	<2		2–10		10–100	>100
IUPAC (2016)[37]	<2				2–50	>50

The coal samples prepared under varying heat treatment temperatures and durations were analysed using an ASAP 2460 analyser, with N_2 as the adsorbate at −195.8 °C. The instrumentation and corresponding technical parameters are detailed in Fig. 2(c) and Table 4.

Under isothermal conditions, the relative pressure was progressively increased. The adsorption and desorption quantities of N_2 were measured at different relative pressures P/P_0 to generate nitrogen adsorption–desorption isotherms. These isotherms were then theoretically analysed to determine pore structure characteristics, including pore morphology, specific surface area, pore volume, and pore size distribution. This method covers a measurable pore size range of 0.4–350 nm, providing accurate characterization of micro- and mesoporous structures in coal.

2.4 Classification of coal pore systems

Coal, as a typical porous medium with dual-porosity systems, exhibits significant heterogeneity and anisotropy. Its internal structure contains abundant matrix pores and microfractures that interconnect the micropores, collectively forming the characteristic dual-porosity architecture of coal. To conduct in-depth research, scholars[27] have classified coal based on the causes of its pores, pore sizes, and connectivity. The specific classification is shown in Table 5.

This study adopts the pore size classification standard established by the International Union of Pure and Applied Chemistry (IUPAC): micropores (<2 nm), mesopores (2–50 nm), and macropores (>50 nm).
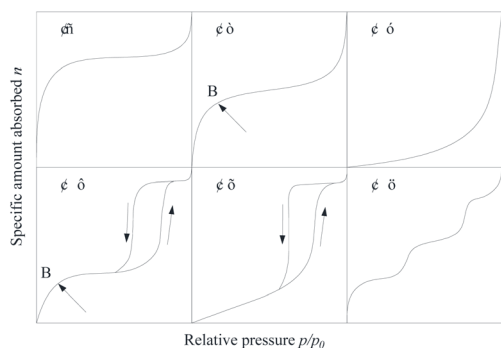

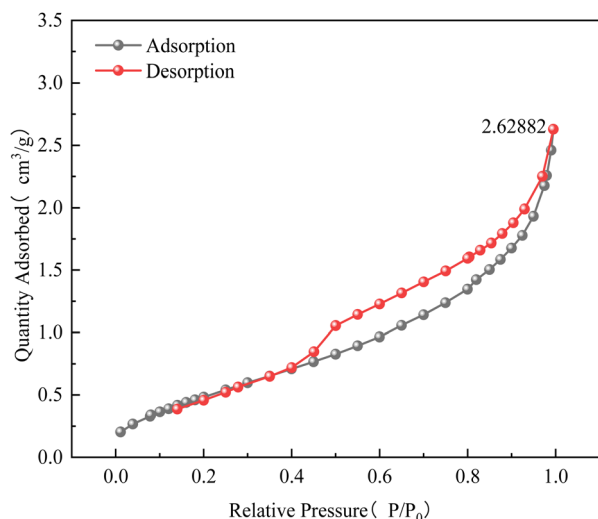**Fig. 3** IUPAC classification of adsorption–desorption isotherms.

3. Result analysis

3.1 Analysis of liquid nitrogen curve and pore types

Distinct types of adsorption–desorption isotherms reveal characteristic features of material behavior during gas uptake and release, enabling the identification and differentiation of various pore structure properties. According to the latest IUPAC classification, these isotherms can be categorized into six distinct types, as shown in Fig. 3.

Due to frequent combustion and even explosive reactions observed in the pure oxygen environment at 170 °C, the oxidation treatment at this preset temperature was not successful. Consequently, only the oxidation treatment processes at 70 °C, 110 °C, and 140 °C were considered in the subsequent analysis and discussion. The pore characteristics of coal samples were characterized through LTNA tests.

The results indicated that the pore diameters of the test coal samples were all within the range of 2 to 50 nm. The adsorption–desorption isotherms of different coal samples are shown
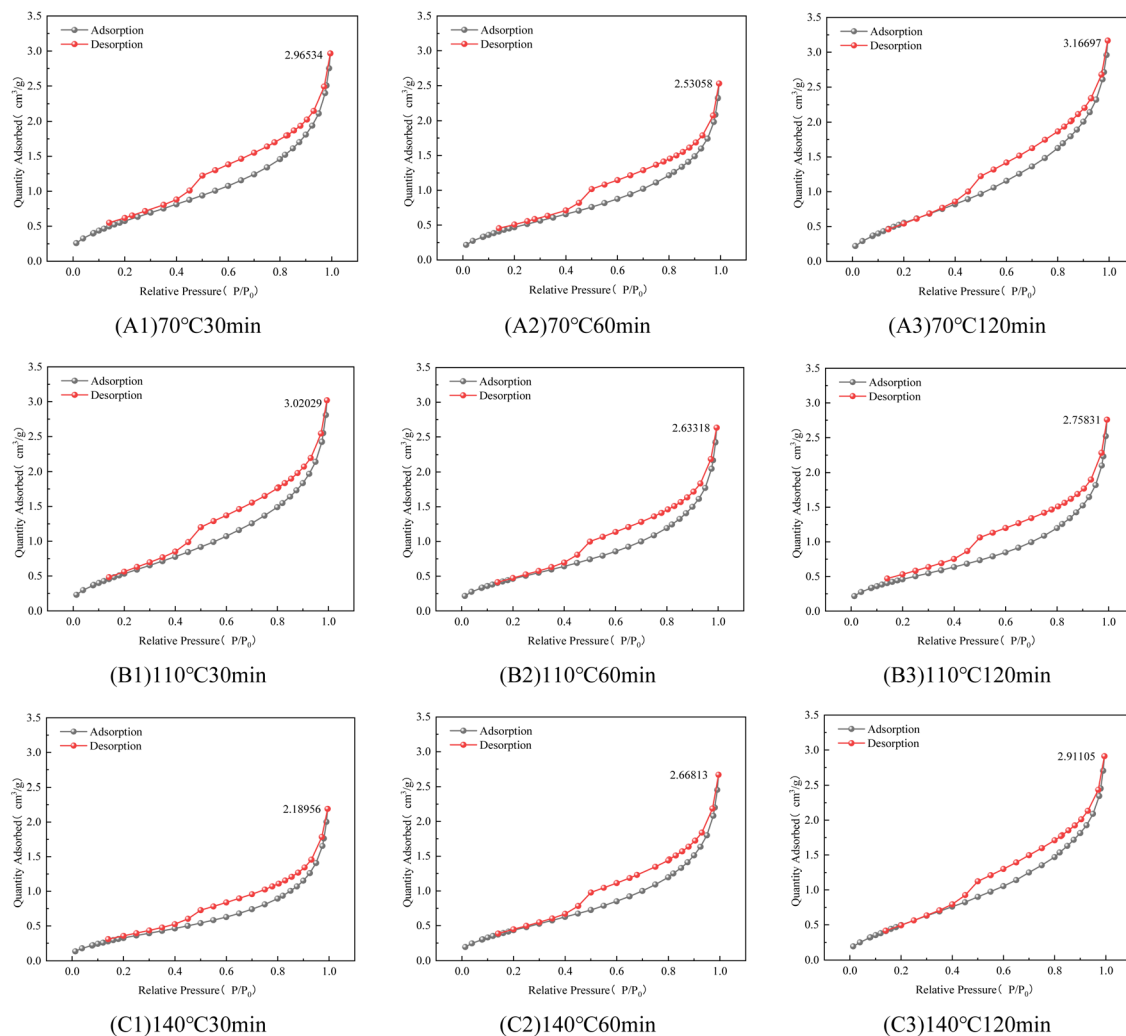

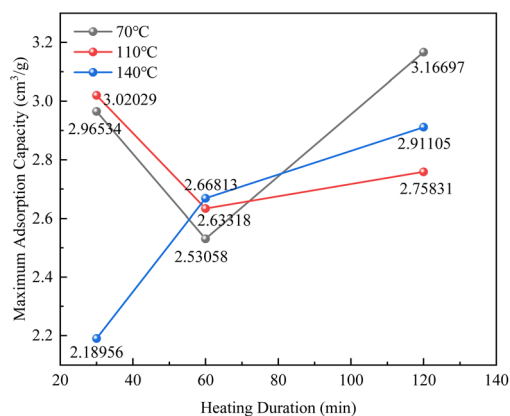
Fig. 4 The adsorption–desorption isotherm of raw coal.

Fig. 5 The adsorption–desorption isotherms of coal samples.

Fig. 6 Temporal variation of liquid nitrogen adsorption capacity in coal at constant temperatures.

a single specific type. By observing and analyzing the adsorption–desorption curves derived from this experiment, the curves of different coal samples presen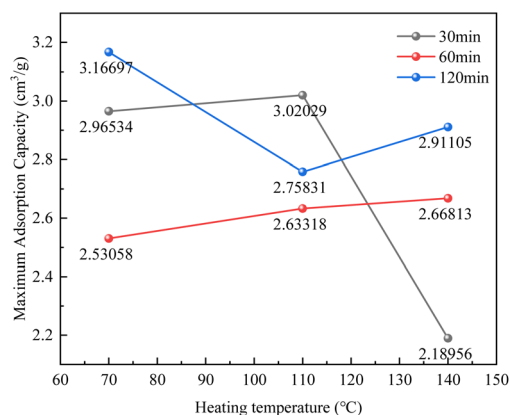ted slight differences in values in Fig. 4 and 5. Due to the complex pore structure of the samples, the adsorption–desorption isotherms obtained from the experiments couldn't be unambiguously classified into

Fig. 7 Time-dependent evolution of maximum N_2 adsorption capacity in coal under isothermal heating.

Table 6 Pore size–volume distribution of coal samples

Coal sample number	Micropore/ (cm³ g⁻¹)	Mesopore/ (cm³ g⁻¹)	Macropore/ (cm³ g⁻¹)	Total pore volume/ (cm³ g⁻¹)	The contribution degree of pore diameter to pore volume/%		
					Proportion of micropores	Proportion of mesopores	Proportion of macropores
R_C	0.000095	0.003323	0.000471	0.003890	2.448	85.441	12.111
A_1	0.000104	0.003684	0.000587	0.004375	2.387	84.199	13.414
A_2	0.000089	0.003035	0.000563	0.003686	2.407	82.330	15.262
A_3	0.000094	0.003948	0.000578	0.004620	2.039	85.441	12.520
B_1	0.000093	0.003707	0.000635	0.004435	2.100	83.585	14.315
B_2	0.000078	0.003135	0.000629	0.003842	2.034	81.594	16.372
B_3	0.000071	0.003218	0.000698	0.003987	1.790	80.716	17.494
C_1	0.000093	0.002482	0.000577	0.003152	2.962	78.735	18.304
C_2	0.000110	0.003142	0.000618	0.003870	2.846	81.193	15.960
C_3	0.000209	0.003405	0.000591	0.004205	4.976	80.976	14.048

and shapes, but the overall trends were similar and approximated type II and type IV isotherms.

Fig. 6 illustrates the maximum liquid nitrogen adsorption capacity of coal samples subjected to different heating durations at fixed temperatures. At 70 °C, the adsorption capacity initially decreased and then increased with prolonged heating time. When the heat treatment temperature reached 110 °C, the adsorption capacity initially decreased, followed by a slight but statistically insignificant increase. At 140 °C, a sustained increase in adsorption capacity was observed, suggesting that thermally induced pore formation predominated over pore collapse or fusion effects at this temperature.

Under fixed time conditions, the maximum liquid nitrogen adsorption capacity of coal samples treated at different heating temperatures is shown in Fig. 7. Significant variations in adsorption capacity were observed with increasing temperature. At a 30-minute heating duration, the maximum adsorption capacity initially increased then decreased with rising temperature. Under 60-minute heating, the adsorption capacity

exhibited a monotonic increase with temperature. In contrast, a 120-minute treatment resulted in an initial decrease followed by an increase in adsorption capacity.

The maximum adsorption capacity of raw coal was measured at 2.62882 cm³ g⁻¹, the value of coal subjected to heat treatment at 70 °C for 30 minutes was 2.96534 cm³ g⁻¹, the value of coal subjected to heat treatment at 110 °C for 60 minutes was 2.63318 cm³ g⁻¹, and the value of coal subjected to heat treatment at 140 °C for 120 minutes was 2.91105 cm³ g⁻¹.

Consequently, the coupled effects of heating temperature and duration exhibit significant interactive influences on liquid nitrogen adsorption capacity, demonstrating a complex trend characterized by an initial increase, followed by a decrease, and subsequent rebound. This phenomenon suggests that heating at 70 °C for 30 minutes likely enhances pore accessibility through mild thermal expansion and surface activation, thereby increasing adsorption capacity. The coal sample treated at 110 °C for 60 minutes exhibited adsorption capacity comparable to
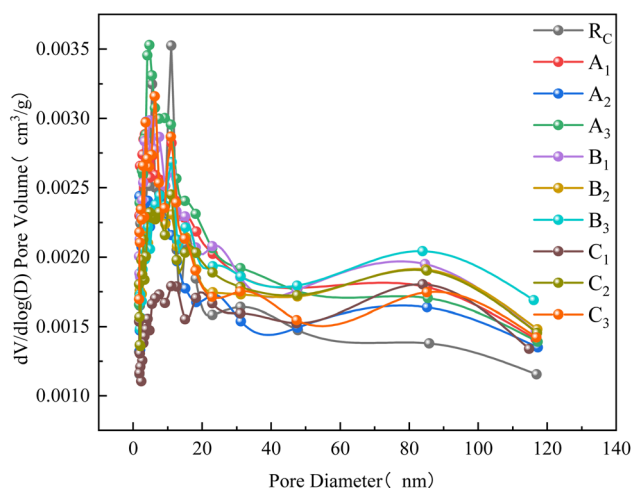

Fig. 8 Different distribution curve of pore size–pore volume of coal samples.
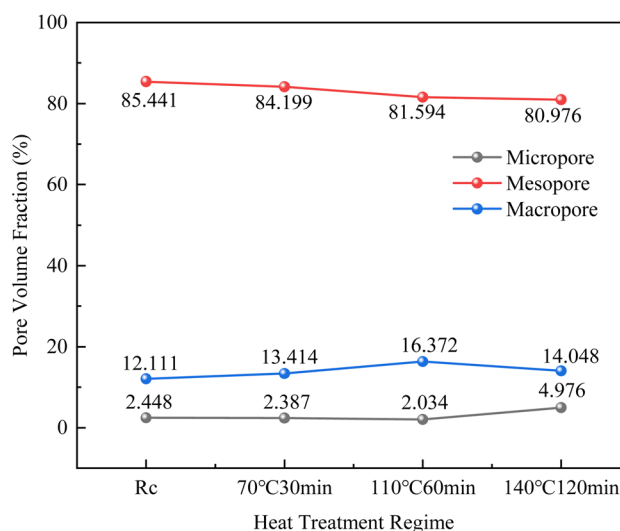

Fig. 9 Nonlinear variation in pore volume proportion.

that of raw coal, suggesting a dual mechanism at play: thermal decomposition generated new micropores while thermal stress simultaneously induced collapse or closure of existing pores. This counterbalancing effect maintained the overall adsorption equilibrium, resulting in similar adsorption capacity to untreated coal. The observed behavior under 140 °C for 120 minutes can be attributed to intensified thermal oxidation, where macromolecular structure cleavage creates new pores while thermal stress-induced pore wall rupture enhances connectivity, collectively improving adsorption performance.

When the relative pressure reaches a critical level, capillary condensation of nitrogen occurs within mesopores, leading to liquefaction. This phenomenon results in greater desorption than adsorption quantities at identical relative pressures, thereby generating hysteresis loops in the isotherm curves. These hysteresis loops typically provide insights into the morphology and structural characteristics of diverse pores within coal samples. According to the 2015 report by the International Union of Pure and Applied Chemistry (IUPAC), scholars have categorized coal pores into four distinct types: cylindrical, slit-shaped, wedge-shaped, and ink-bottle pores.[38]

At low relative pressures ($P/P_0 < 0.1$), the adsorption curve exhibited a rapid initial rise with slight upward convexity, indicating micropore filling and monolayer adsorption on the material surface. At this stage the micropores were filled, adsorption occurred mainly on the surface of the material, and monolayer adsorption tended to be saturated at the inflection point. Multilayer adsorption commences within the relative pressure range of 0.1 to 0.8 (P/P_0). Nitrogen undergoes capillary condensation within mesopores, transitioning into liquid nitrogen and giving rise to a hysteresis loop. When the relative pressure exceeds 0.8, capillary condensation progressively extends to larger mesopores, thereby resulting in gas condensation in capillary pores of larger diameters and a rapid increase in the adsorption capacity, which is similar to the high relative pressure stage of type II isotherms.

According to the Kelvin formula,[39] the pore size exhibits a positive correlation with relative pressure. Specifically, at relative pressures of 0.4, 0.5, and 0.8, the corresponding pore diameters are approximately 3.3 nm, 4 nm, and 10 nm, respectively.

At relative pressures below 0.4 ($P/P_0 < 0.4$), the adsorption–desorption curves basically overlapped, indicating that pores smaller than 3.3 nm are predominantly dead-end pores. In the relative pressure range of $0.4 < P/P_0 < 1.0$, a pronounced hysteresis loop is observed, suggesting the presence of inter-connected mesopores (>3.3 nm) with diverse geometries, including cylindrical open-ended pores, slit-shaped pores, and ink-bottle pores with narrow necks.

At a relative pressure of approximately 0.5 ($P/P_0 \approx 0.5$), a notable inflection point emerged on the desorption isotherm, accompanied by a considerable decline, reveals that the pore size distribution between 3.3 and 4 nanometers is primarily dominated by ink-bottle-shaped pores. Compared with the raw coal, heating treatment didn't alter the adsorption–desorption hysteresis loops of the coal specimens, indicating that the pore structure of this shape is stable, and heat treatment doesn't cause significant changes in the pore shape.

3.2 Characteristics of pore volume and pore size distribution

This study employed the BET and BJH models to characterize mesoporous structures and analyze pore structure evolution in coal samples subjected to heat treatment at varying temperatures. The pore size distribution and corresponding pore volume contribution of the sample, as determined by the BJH method, are presented in Table 6. The pore size distribution curve is presented in Fig. 8.

As shown in Fig. 8, mesopores were well developed in all coal samples, showing similar pore volume distribution patterns. Multiple peaks appeared in the 2–50 nm pore diameter range, followed by a single peak at 80–90 nm. The pore size and volume distribution data indicate that the total pore volume of the coal samples ranges from 0.003152 cm^3 g^{-1} to 0.004620 cm^3 g^{-1}. Among them, the micropore volume is between 0.000071 cm^3 g^{-1} and 0.000209 cm^3 g^{-1}, with a contribution rate of 1.790% to 4.976%; the mesopore volume is between 0.002482 cm^3 g^{-1} and

Table 7 Pore size−surface area distribution of coal samples

| Coal sample number | Micropore/ (m^2 g^{-1}) | Mesopore/ (m^2 g^{-1}) | Macropore/ (m^2 g^{-1}) | Total surface area/ (m^2 g^{-1}) | BET surface area/ (m^2 g^{-1}) | The contribution degree of pore diameter to surface area/% | | |
						Proportion of micropores	Proportion of mesopores	Proportion of macropores
R_C	0.000000	0.819007	0.011526	0.8305	1.9708	0.000	98.612	1.388
A_1	0.025332	0.716090	0.008579	0.7500	2.3053	3.378	95.479	1.144
A_2	0.026101	0.509686	0.007106	0.5428	1.8557	4.808	93.883	1.309
A_3	0.000000	1.155724	0.021804	1.1775	2.3173	0.000	98.148	1.852
B_1	0.000000	0.818975	0.014072	0.8330	2.1630	0.000	98.311	1.689
B_2	0.036379	0.476011	0.009284	0.5217	1.8035	6.974	91.247	1.780
B_3	0.015881	0.420983	0.009205	0.4461	1.7830	3.560	94.376	2.063
C_1	0.000000	0.521419	0.016613	0.5380	1.3440	0.000	96.912	3.088
C_2	0.000000	0.603932	0.013495	0.6174	1.7371	0.000	97.814	2.186
C_3	0.000000	1.046977	0.021742	1.0687	2.1595	0.000	97.966	2.034
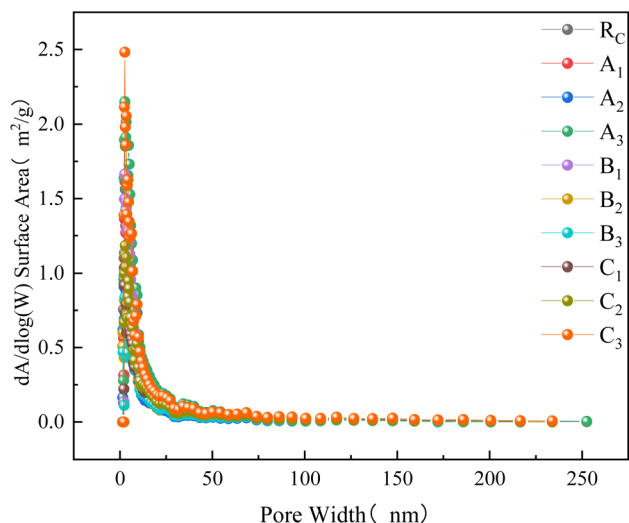
Fig. 10 Different distribution curve of pore size–surface area of coal samples.

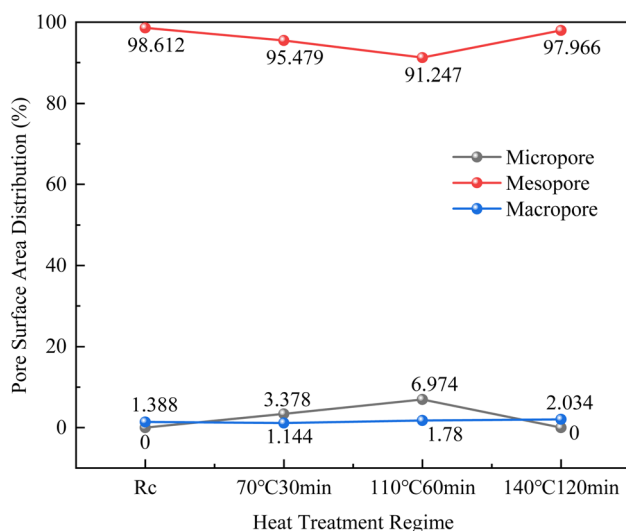**Fig. 11** Nonlinear variation in surface area fraction.

0.003948 cm^3 g^{-1}, with a contribution rate of 78.735% to 85.441%; and the macropore volume ranges from 0.000471 to 0.000698 cm^3 g^{-1}, accounting for 12.111% to 18.304%. These results demonstrate that mesopores constituted the dominant pore system, followed by macropores, with micropores making the smallest contribution to the total pore volume.

As shown in Fig. 9, with increasing heating temperature and duration, the proportion of mesopores to total pore volume gradually decreased from 85.441% to 80.976%. In contrast, the proportion of micropores initially declined from 2.448% to 2.034%, then increased to 4.976%, while macropores first rose from 12.111% to 16.372% before decreasing to 14.048%. Overall, both micropores and macropores exhibited a net increase in their proportional contributions.

3.3 Characteristics of pore specific surface area and pore size distribution

The distribution data of pore size and specific surface area of the statistical samples, as well as the contribution of pore size to pore volume, are shown in Table 7. The variation of specific surface area with pore size distribution is presented in Fig. 10.

As shown in Fig. 10, all samples demonstrate similar trends in specific surface area variation as a function of pore size distribution. Each sample exhibits a unimodal peak in the pore size range of 2–5 nm, followed by a gradual decrease in specific surface area with increasing pore diameter.

The BET specific surface area of the coal samples ranged from 1.3440 to 2.3173 m^2 g^{-1}. Among them, the surface area of micropores ranges from 0 to 0.036379 m^2 g^{-1}, accounting for 0% to 6.974% of the total surface area. The surface area of mesopores is between 0.420983 m^2 g^{-1} and 1.155724 m^2 g^{-1}, and the contribution ratio reaches 91.247% to 98.612%. Macropores exhibit a specific surface area between 0.007106 and 0.021804 m^2 g^{-1}, accounting for 1.144% to 3.088% of the total surface area.

As shown in Fig. 11, the proportion of micropores to total surface area exhibited a unimodal trend, initially increasing from 0% to a peak of 6.974%, then decreasing back to 0%. The proportions occupied by mesopores and macropores demonstrate a pattern of first declining and then ascending. The proportion of mesopores reduces from 98.612% to 91.247%

Table 8 Fractal dimension analysis of coal samples

Coal sample number	Low-pressure region (0 < P/P_0 < 0.5)			High-pressure region (0.5 < P/P_0 < 1.0)		
	A$_1$	D$_1$	R$_1^2$	A$_2$	D$_2$	R$_2^2$
R$_C$	−0.22419	2.77581	0.93491	−0.75226	2.24774	0.99154
A$_1$	−0.23056	2.76944	0.95891	−0.70360	2.29640	0.99030
A$_2$	−0.23788	2.76212	0.96140	−0.67727	2.32273	0.99076
A$_3$	−0.22699	2.77301	0.93552	−0.79959	2.20041	0.99156
B$_1$	−0.23499	2.76501	0.95352	−0.74703	2.25297	0.99324
B$_2$	−0.25587	2.74413	0.96589	−0.65950	2.34050	0.99130
B$_3$	−0.26977	2.73023	0.96791	−0.64900	2.35100	0.99088
C$_1$	−0.28690	2.71310	0.97114	−0.75094	2.24906	0.98580
C$_2$	−0.26015	2.73985	0.96255	−0.72284	2.27716	0.99217
C$_3$	−0.22713	2.77287	0.94450	−0.85336	2.14664	0.99127
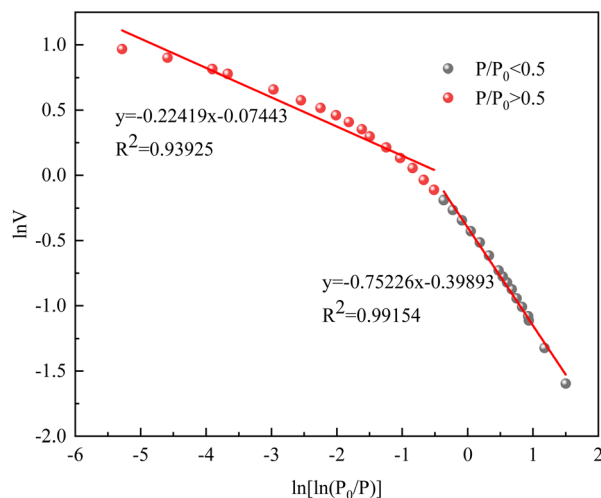
Fig. 12 Fractal dimension fitting plot of raw coal scatter data.

3.4 Pore fractal characteristics

Fractal geometry quantifies the complexity and surface roughness of coal pore structures through fractal dimension analysis. When determining the fractal dimension of coal using LTNA tests, the FHH model based on multilayer adsorption theory is commonly employed.

Based on distinct adsorption mechanisms, the isotherm was divided into two characteristic regions: the low-pressure region ($P/P_0 < 0.5$), where fractal dimension D_1 was derived from fitting; and the high-pressure region ($P/P_0 > 0.5$), yielding fractal dimension D_2 through fitting analysis. The calculated results are presented in Table 8 and Fig. 12 and 13.

According to fractal geometry theory, the fractal dimension D should range between 2 and 3. As an effective quantitative indicator of pore structure evolution, variations in D directly reflect the regulatory effects of both temperature and duration during pyrolysis. Previous studies[40] have shown that the D_1 parameter serves as an effective indicator of coal surface roughness, where a higher value corresponds to increased surface irregularity and enhanced gas adsorption capacity. D_2 reflects the structural complexity of coal pores, with increased

and then increases to 97.966%, while the proportion of macropores decreases from 1.388% to 1.144% and then rises to 2.034%.
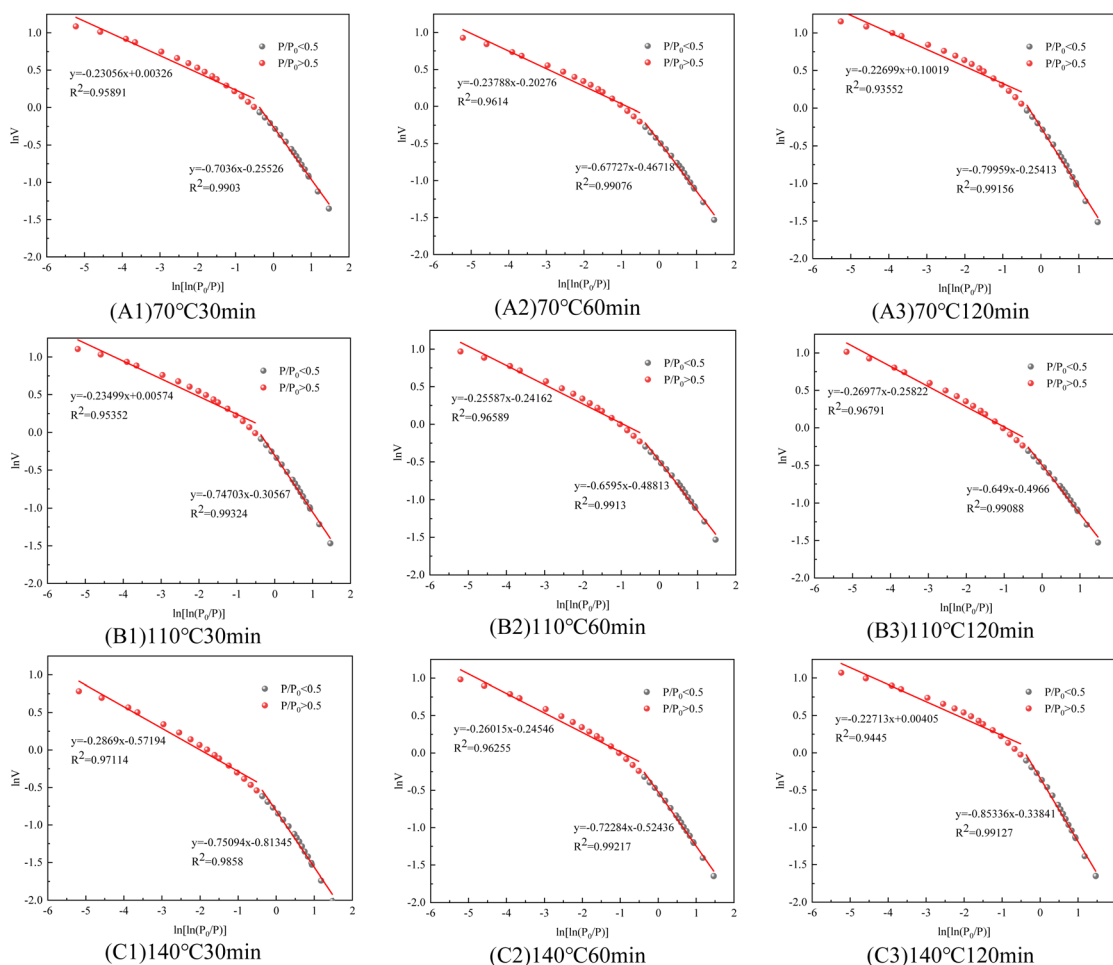

Fig. 13 Fractal dimension fitting plot of coal samples.

values denoting greater pore heterogeneity and reduced adsorption performance.

Analysis of Table 8 data reveals that under constant heating duration, both D_1 and D_2 exhibit decreasing trends with rising temperature. This systematic variation indicates that elevated temperatures induce partial closure or collapse of micropores and mesopores, leading to the formation of larger pores. Consequently, the pore structure becomes simplified, with reduced complexity and roughness, while simultaneously enhancing connectivity and permeability.

The temporal effect exhibits more complex non-monotonic characteristics. Under constant temperatures of 70 °C and 140 °C, prolonged heating duration resulted in an initial decrease followed by an increase in low-pressure region D_1, while high-pressure region D_2 exhibited an opposite trend. During the initial heating stage, organic matter pyrolysis led to partial micropore closure and generation of new mesopores. With extended heating duration, pore evolution was dominated by micropore regeneration and pore channel coalescence. In contrast, under a constant temperature of 110 °C, D_1 showed continuous decrease while D_2 increased steadily, suggesting this temperature may represent a critical threshold between pore contraction and generation mechanisms.

Under coupled time–temperature effects, the initial stage showed a decrease in low-pressure region D_1 and an increase in high-pressure region D_2, indicating partial micropore closure and mesopore formation in coal samples. Under thermal treatment at 140 °C for 120 minutes, D_1 increased to 2.77287 while D_2 decreased to 2.14664, indicating the formation of secondary pores and the collapse of original pore channels during prolonged high-temperature pyrolysis.

4. Conclusions

This study conducted thermal treatment of coal samples at varying temperatures and durations using oil-bath low-temperature oxidation experiments. The pore structure was subsequently characterized through LTNA tests. In combination with the FHH fractal theory, the fractal dimension of the coal body was calculated and analyzed, and the following conclusions were obtained:

(1) With increasing thermal treatment temperature and duration, the overall shape of the coal's adsorption–desorption isotherms remained stable without significant alterations, exhibiting characteristics intermediate between Type II and Type IV isotherms. Within the experimental parameter range, no substantial reconstruction of the coal pore structure was observed, though diverse pore morphologies were identified, including closed-end ink-bottle pores and various open meso-pores (cylindrical and slit-shaped). While open mesopores facilitated gas diffusion, closed pores likely contributed to gas entrapment. This dual effect significantly influenced the liquid nitrogen adsorption curves.

(2) With increasing heating temperature and duration, the mesopore volume fraction decreased progressively from 85.441% to 80.976%. In contrast, the micropore fraction initially declined from 2.448% to 2.034%, then increased to 4.976%, while the macropore fraction first rose from 12.111% to 16.672% before decreasing to 14.048%, showing an overall upward trend. Regarding specific surface area distribution, the micropore contribution initially increased from 0% to 6.974% before returning to 0%. Both mesopores and macropores exhibited a decreasing-then-increasing pattern: mesopores decreased from 98.612% to 91.247% before recovering to 97.966%, whereas macropores reduced from 1.388% to 1.144% then rebounded to 2.034%.

(3) The high goodness-of-fit of the curves indicates distinct stage-specific fractal characteristics in the pore structure. Under the same heating time, the increase in heating temperature lead to decreased D_1 and D_2 values, suggesting progressive simplification of the pore architecture. Under isothermal conditions, fractal dimension D_1 exhibited an initial decrease followed by an increase over time, while D_2 displayed the opposite trend. This inverse relationship reflects the dynamic evolution of pore structures under thermal variations, corresponding to the competing mechanisms of thermal cracking and oxidation reactions.

(4) The observed alterations in pore structure suggest that thermal treatment preferentially modifies mesoporous structures, with potential pore coalescence or collapse occurring at elevated temperatures. However, the temperature range investigated in this study differs from actual coal spontaneous combustion conditions, necessitating future research at higher temperatures.

Author contributions

Yaxian Yu: writing – original draft, conceptualization, investigation, formal analysis, visualization, validation, data curation; Zhenya Zhang: writing – review & editing, supervision, methodology, funding acquisition, conceptualization; Song Kong: supervision, funding acquisition; Peitao Zhu: formal analysis, supervision, investigation.

Conflicts of interest

The authors declare that they have no known competing financial interests or personal relationships that could have appeared to influence the work reported in this paper.

Data availability

All relevant data are within the paper.

Acknowledgements

References

1 H. Fu, K. Yuan, S. Lu, X. Chen, T. Lin, S. Du, B. He and X. Luo, Microscopic pore structure characteristics and its effect on gas-bearing property of high-rank coal in Upper Permian Longtan Formation in western Guizhou, *Nat. Gas Geosci.*, 2020, **31**, 1814–1825.

2 Y. Shen, X. Wang, C. Zhao, S. Wang, C. Guo, Q. Shi and W. Ma, Experimental study on multi-scale pore structure characteristics of tar-rich coal in Yushenfu mining area, *Coal Geol. Explor.*, 2021, **49**, 33–41.

3 T. Li, C. Wu and Z. Wang, Isothermal characteristics of methane adsorption and changes in the pore structure before and after methane adsorption with high-rank coal, *Energy Explor. Exploit.*, 2020, **38**, 1409–1427.

4 F. Yang, D. He, D. Ma, Z. Duan, T. Tian and D. Fu, Multi-scale joint characterization of micro-pore structure of low-rank coal reservoir, *Lithol. Reservoirs*, 2020, **32**, 14–23.

5 S. Xu, E. Hu, X. Li and Y. Xu, Quantitative analysis of pore structure and its impact on methane adsorption capacity of coal, *Nat. Resour. Res.*, 2021, **30**, 605–620.

6 H. Xue, X. Li, L. Chen and Y. Liu, Micropore fractal characteristics of outburst coal in Western Guizhou and its influence on permeability, *Coal Sci. Technol.*, 2021, **49**, 118–122.

7 J. Liu, S. Wang and D. Su, Study on pore development characteristics of low rank coal reservoirs in Erlian Basin group, *Saf. Coal Mine*, 2021, **52**, 7–12.

8 F. Gao, Y. Song, Z. Liang, Z. Li, Y. Yuan, Y. Zhang, L. Chen and W. Guo, Development characteristics of organic pore in the continental shale and its genetic mechanism: a case study of Shahezi Formation shale in the Changling fault depression of Songliao Basin, *Acta Pet. Sin.*, 2019, **40**, 1030–1044.

9 K. Zhang, Z. Meng, Y. Jin and B. Wang, Fractal characteristics of pore structures on different coal structures and its research significance, *Coal Sci. Technol.*, 2023, **51**, 198–206.

10 L. Shao, J. Li, S. Wang, H. Hou, J. Li and M. Zhu, Pore structures and fractal characteristics of liquid nitrogen adsorption pores in lignite in the Hailar Basin, *Nat. Gas. Ind.*, 2020, **40**, 15–25.

11 S. Zhou, D. Liu, Y. Cai, Y. Yao, Y. Jiao and S. Ren, Characterization and fractal nature of adsorption pores in low rank coal, *Oil Gas Geol.*, 2018, **39**, 373–383.

12 Q. Li, Y. Wu and L. Qiao, Combined characterization of pore structure in deep medium-rank coal using mercury intrusion and liquid nitrogen adsorption methods and its pore fractal characteristics, *Exp. Pet. Geol.*, 2025, **47**, 130–142.

13 Y. Liu, X. Zhang and J. Miao, Study on evolution of pore structure of medium and high rank coals, *Saf. Coal Mine*, 2020, **51**, 7–13.

14 M. Zhang, L. Zhang, Q. Zhao, L. Si, C. Wang, J. Lin and G. Wu, Study on pore structure and fractal characteristics of high-rank coals in Southwest Guizhou based on mercury intrusion and N_2 adsorption, *Coal Geol. China*, 2025, **37**, 1–8.

15 Z. Yin, H. Xu, D. Tang, Y. Chen and T. Zhao, Study on pore structure change during different coal grade pyrolysis, *Coal Sci. Technol.*, 2019, **47**, 74–79.

16 Z. Zhang, Q. Qian, Y. Chen and C. Tang, Study on the effects of high-pressure CO_2 adsorption/desorption on the pore structure of bituminous coal, *J. Saf. Environ.*, 2025, **25**, 108–120.

17 D. Zhao, Y. Guo, G. Wang and X. Mao, Characterizing nanoscale pores and its structure in coal: Experimental investigation, *Energy Explor. Exploit.*, 2019, **37**, 1320–1347.

18 L. Qi, X. Zhou, X. Peng, Z. Wang and J. Dao, Study on pore structure of coking coal based on low-temperature nitrogen adsorption and mercury intrusion method, *Saf. Coal Mine*, 2022, **53**, 1–6.

19 Y. Lin, X. Jia and D. Ma, Study and application of coal pore features based on liquid nitrogen adsorption method, *Coal Sci. Technol.*, 2016, **44**, 135–140.

20 H. Li, S. Shi, J. Lu, Q. Ye, Y. Lu and X. Zhu, Pore structure and multifractal analysis of coal subjected to microwave heating, *Powder Technol.*, 2019, **346**, 97–108.

21 Y. Cui, Y. Hu, Y. Song, J. Feng and W. Li, Pore evolution and its influence on volatile mass transfer during long-flame coal pyrolysis, *CIESC J.*, 2025, 1–16.

22 C. Zhou, X. Chen, Y. Zhang and Z. Wan, Study on pore evolution and porous elastoplastic deformation characteristics of anthracite after high temperature, *China Min. Mag.*, 2022, **31**, 165–172.

23 S. Zhang, S. Tang, D. Tang, W. Huang and Z. Pan, Determining fractal dimensions of coal pores by FHH model: Problems and effects, *J. Nat. Gas Sci. Eng.*, 2014, **21**, 929–939.

24 X. Wang, S. Yin, M. Cao, M. Xia, D. Liu, J. Zhang, C. Wu, Q. LI, H. Wang and R. Lu, Microscopic pore of sandstone in Longde Coal Mine based on FHH fractal theory, *Saf. Coal Mine*, 2024, **55**, 179–189.

25 Z. Wang, Y. Cheng, Y. Qi, R. Wang, L. Wang and J. Jiang, Experimental study of pore structure and fractal characteristics of pulverized intact coal and tectonic coal by low temperature nitrogen adsorption, *Powder Technol.*, 2019, **350**, 15–25.

26 C. Duan, X. Fu, Z. Deng, J. Kang, B. Zhang, J. Lu, X. Hong, R. Dai and X. Li, Pore structure multifractal characteristics of coal reservoirs in the central and eastern Qinshui Basin and influencing Factors, *Processes*, 2023, **11**, 286.

27 Y. Cheng and B. Hu, A new pore classification method based on the methane occurrence and migration characteristics in coal, *J. China Soc.*, 2023, **48**, 212–225.

28 B. B. Hodot, *Outburst of Coal and Coalbed Gas (Chinese Translation)*, Chemical Industry Press, Beijing, 1966.

29 H. Gan, S. P. Nandi and P. L. Walker, Nature of the porosity in American coals, *Fuel*, 1972, **51**, 272–277.

30 M. M. Dubinin, On physical feasibility of Brunauer's micropore analysis method, *J. Colloid Interface Sci.*, 1974, **46**, 351–356.

31 J. Wu, K. Jin, Y. Tong and R. Qian, Pore theory of coal and its application in the evaluation of gas outburst and drainage, *J. Colloid Interface Sci.*, 1991, 86–95.

32 C. Liu, An experimental study on the pore structure characteristics of coal, *Coal Mine Saf.*, 1993, 1–5+49.

33 Y. Qin, Z. Xu and J. Zhang, Natural classification of the high-rank coal pore structure and its application, *J. Colloid Interface Sci.*, 1995, 266–271.

34 X. Fu, Y. Qin, W. Zhang, C. Wei and R. Zhou, Fractal classification and natural classification of coal pores based on coalbed methane migration, *Sci. Bull.*, 2005, 51–55.

35 Y. Ju, B. Jiang, Q. Hou, G. Wang and A. Fang, Structural evolution of nano-scale pores of tectonic coals in southern north china and its Mechanism, *Acta Geol. Sin.*, 2005, 269–285.

36 S. Sang, M. Zhu, S. Zhang, J. Zhang and J. Tang, Solid-gas interaction mechanism of coal-adsorbed gas(I)—Coal pore structure and solid-gas interaction, *Nat. Gas. Ind.*, 2005, 13–15.

37 M. Thommes, K. Kaneko, A. V. Neimark, J. P. Olivier, F. Rodriguez-Reinoso, J. Rouquerol and K. S. W. Sing, Physisorption of gases, with special reference to the evaluation of surface area and pore size distribution (IUPAC Technical Report), *Pure Appl. Chem.*, 2015, **87**, 1051–1069.

38 X. Li, Z. Li, L. Zhang, J. Gao, B. Nie and Y. Meng, Pore structure characterization of various rank coals and its effect on gas desorption and diffusion, *J. Colloid Interface Sci.*, 2019, **44**, 142–156.

39 L. Bao, P. Gao and S. Peng, Analysis method of pore size distribution of porous materials, *Mater. Sci.*, 2020, **10**, 95–103.

40 J. Liu, Y. Zhang, D. Yang, Z. Gao and D. Wang, Joint characterization of middle and low rank coal pores and fractures based on pressed mercury-nitrogen adsorption-nuclear magnetic resonance method, *J. Henan Polytech. Univ., Nat. Sci.*, 2025, **44**, 19–31.